nature physics

Charge noise and spin noise in a semiconductor quantum device

Andreas V. Kuhlmann[1]*, Julien Houel[1], Arne Ludwig[1,2], Lukas Greuter[1], Dirk Reuter[2,3], Andreas D. Wieck[2], Martino Poggio[1] and Richard J. Warburton[1]

Improving the quantum coherence of solid-state systems that mimic two-level atoms, for instance spin qubits or single-photon emitters using semiconductor quantum dots, involves dealing with the noise inherent to the device. Charge noise results in a fluctuating electric field, spin noise in a fluctuating magnetic field at the location of the qubit, and both can lead to dephasing and decoherence of optical and spin states. We investigate noise in an ultrapure semiconductor device using a minimally invasive, ultrasensitive local probe: resonance fluorescence from a single quantum dot. We distinguish between charge noise and spin noise through a crucial difference in their optical signatures. Noise spectra for both electric and magnetic fields are derived from 0.1 Hz to 100 kHz. The charge noise dominates at low frequencies, spin noise at high frequencies. The noise falls rapidly with increasing frequency, allowing us to demonstrate transform-limited quantum-dot optical linewidths by operating the device above 50 kHz.

Semiconductor quantum dots are hosts for spin qubits[1,2]. Optically active quantum dots, for instance self-assembled quantum dots, are in addition potentially excellent single-photon sources[3]. Optimizing performance demands an understanding of noise and a strategy to circumvent its deleterious effects[4]. There are two main sources of noise in a semiconductor. Charge noise arises from occupation fluctuations of the available states and leads to fluctuations in the local electric field. This results in shifts in the optical transition energy of a quantum dot through the d.c. Stark effect and is one mechanism by which the optical linewidth of a self-assembled quantum dot can be significantly increased above the transform limit[5–7]. Charge noise can also result in spin dephasing through the spin–orbit interaction, and, in particular for hole spins, through the electric field dependence of the g-factor[8,9]. The second source of noise, spin noise, arises typically from fluctuations in the nuclear spins of the host material and, on account of the hyperfine interaction, results in a fluctuating magnetic field (the Overhauser field) experienced by an electron spin[10,11]. Spin noise from noisy nuclei results in rapid spin dephasing in an InGaAs quantum dot[12–14].

Strategies for reducing noise involve working with ultraclean materials to minimize charge noise, and possibly nuclear-spin-free materials to eliminate spin noise. Abandoning GaAs comes however with a significant loss of flexibility for both spin qubits and quantum photonics applications. A second powerful paradigm is the use of dynamic decoupling, schemes that employ complex echo-like sequences to protect the qubit from environmental fluctuations[15–17]. In this case, it is absolutely crucial that the noise power decreases with increasing frequency.

For quantum-dot-based single photon sources, the linewidths are in the best case (high-quality material with resonant excitation) typically about a factor of two larger than the transform limit in which the linewidth is determined only by the radiative decay time[5–7]. This is a poor state of affairs for applications that rely on photon indistinguishability, the resource underpinning a quantum repeater for instance. On the positive side, there

is evidence that with low-power, resonant excitation, there is no significant upper-level dephasing apart from radiative recombination[18,19]. It has been surmised that the increase in linewidth above the ideal limit arises from a spectral wandering[5,7] but the origin of the noise and its frequency dependence has not been pinned down. Concerning spin qubits, untreated noisy nuclei limit the electron spin coherence qubit[10,11]. However, the mesoscopic nature—a quantum dot contains 10^5–10^6 nuclear spins—allows the nuclear spins to be manipulated, both quietened down and polarized[20].

Some progress has been made in understanding noise in semiconductor quantum devices. In the context of quantum transport, a spin noise spectrum has been deduced at high frequencies from the time dependence of spin qubit dynamic decoupling[21], and at low frequencies from successive spin qubit readout operations[22], leaving a gap at intermediate frequencies[23]. A spin noise spectrum has also been determined through the Faraday rotation of a detuned laser on an ensemble of quantum dots[24] but not at the local, single-quantum-dot level.

We present here an investigation of noise in an ultraclean semiconductor quantum device, using a minimally invasive, ultrasensitive, local probe: resonance fluorescence (RF) from a single quantum dot (Fig. 1a, see Methods). We present noise spectra with 6 decades of resolution in the noise power over 6 decades of frequency, from 0.1 Hz to 100 kHz (Fig. 2a,b). Significantly, we have discovered a spectroscopic way to distinguish charge noise from spin noise (Fig. 3). We find that the charge noise gives large noise powers but only at low frequencies. The spin noise gives much weaker noise powers but over a much larger bandwidth. Remarkably, our experiment is able to reveal the full spectrum of the fluctuating nuclear spin ensemble. We translate the RF noise spectrum into two separate noise spectra, one for the local electric field (charge noise) and one for the local magnetic field (spin noise). The charge noise spectrum is Lorentzian with a small $1/f$-like component; the spin noise spectrum is purely Lorentzian, falling as $1/f^2$ at high frequency. The combined noise

[1]Department of Physics, University of Basel, Klingelbergstrasse 82, CH-4056 Basel, Switzerland, [2]Lehrstuhl für Angewandte Festkörperphysik, Ruhr-Universität Bochum, D-44780 Bochum, Germany, [3]Department Physik, Universität Paderborn, Warburger Strasse 100, D-33098 Paderborn, Germany. *e-mail: andreas.kuhlmann@unibas.ch
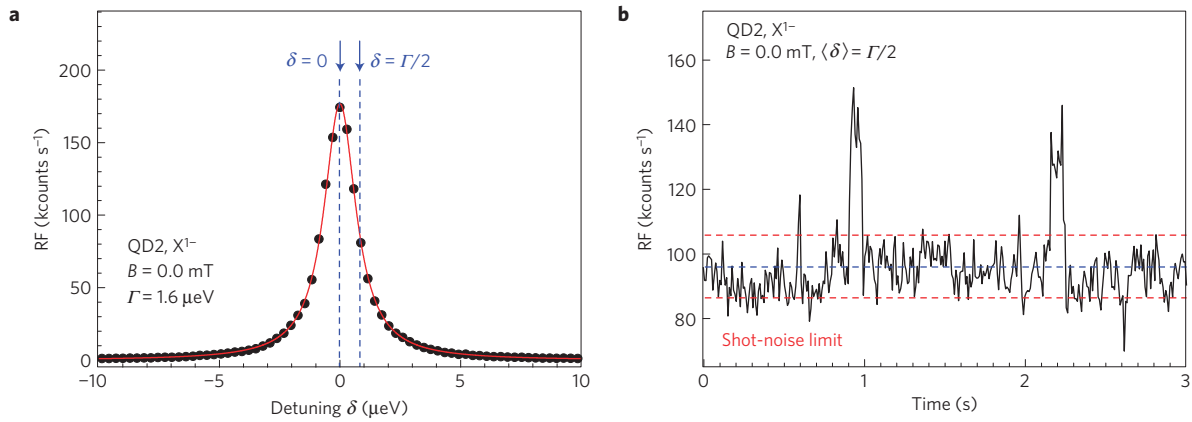
Figure 1 | RF on a single quantum dot. a, RF recorded on a single InGaAs quantum dot, QD2, at a wavelength of 950.61 nm at a power corresponding to a Rabi energy of 0.55 µeV at a temperature of 4.2 K without an external magnetic field. The RF was detected with a silicon avalanche photodiode operating in single-photon mode; the detuning was achieved by sweeping the gate voltage with respect to the laser using the d.c. Stark effect. In this case, the integration time per point was 100 ms. The solid line is a Lorentzian fit to the data with linewidth $\Gamma = 1.6$ µeV (390 MHz). **b**, A time trace of the RF recorded with detuning set to half the linewidth, $\langle \delta \rangle = \Gamma/2$. The arrival time of each detected photon is stored, allowing a time trace to be constructed post-experiment with an arbitrary binning time. An example is shown using a binning time of 10 ms.
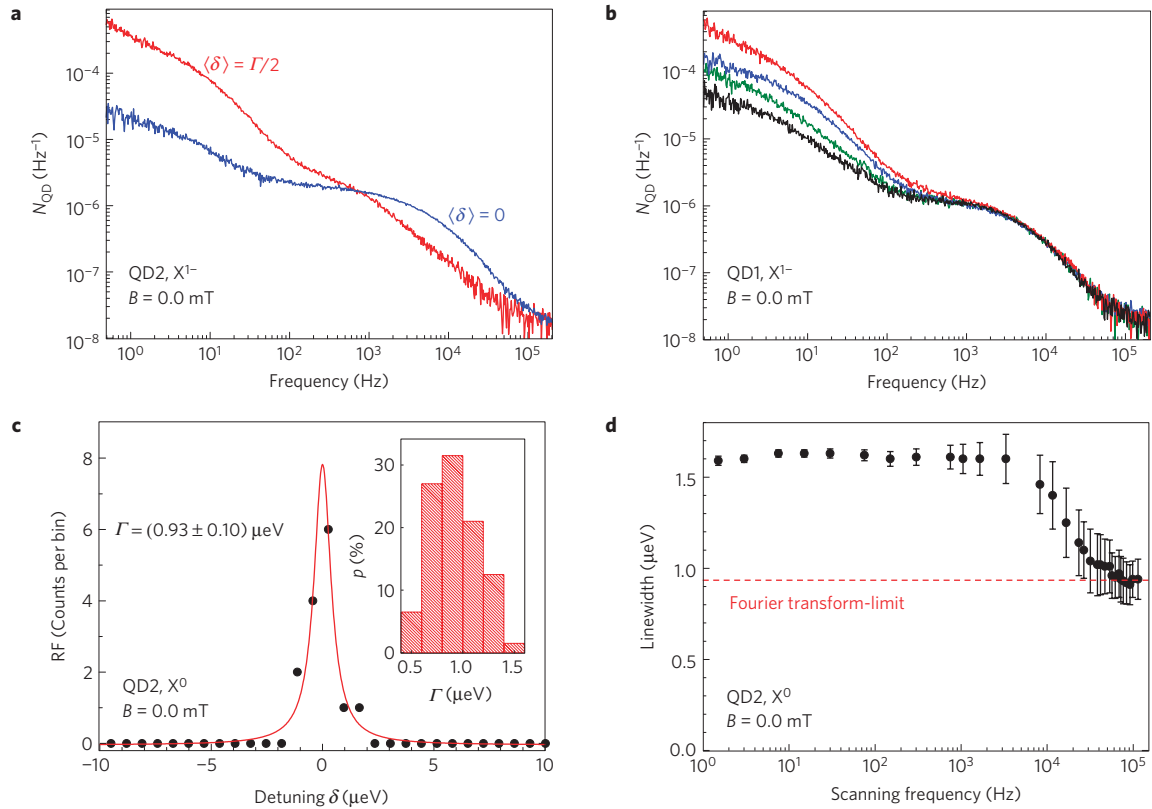
Figure 2 | RF noise. a, RF noise spectra recorded on a quantum dot (the one from Fig. 1, QD2) occupied with a single electron, the trion X^{1-}, for average detuning equal to zero, $\langle \delta \rangle = 0$ (blue), and for $\langle \delta \rangle = \Gamma/2$ (red) at 4.2 K and $B = 0.0$ mT. Following the scheme in Fig. 3, the noise at low frequencies is shown to originate from charge noise, that at high frequencies from spin noise. Plotted is the noise power spectrum of the normalized RF, $S(t)/\langle S(t) \rangle$, where $S(t)$ is the RF signal, and $\langle S(t) \rangle$ is the average RF signal, corrected for external sources of noise (see Supplementary Information). **b**, RF noise spectra recorded on X^{1-} with $\langle \delta \rangle = 0$ under identical experimental conditions (4.2 K, $B = 0.0$ mT) in the course of the experiment. The charge noise at low frequency depends on the sample history; the spin noise at high frequency does not. **c**, An example X^0 RF spectrum measured with $f_{scan} = 58$ kHz and 13 µs binning time. The scanning frequency is defined as $d\delta/dt/\Gamma_0$, where Γ_0 is the transform-limited linewidth. Inset: histogram of 200 linewidths recorded also with $f_{scan} = 58$ kHz. **d**, RF linewidth against scanning frequency. The radiative lifetime is $\tau_r = (700 \pm 50)$ ps. Γ approaches Γ_0 for scanning frequencies above 50 kHz. For each f_{scan}, the error bar represents the standard deviation of several hundred linewidth scans.

falls rapidly with frequency becoming insignificant above 50 kHz for the quantum-dot optical transition as signalled by transform-limited linewidths.

A typical time trace of the RF is shown in Fig. 1b with a binning time of 10 ms. At first sight, one might think that the time trace is unlikely to be very revealing about the local environmental noise as
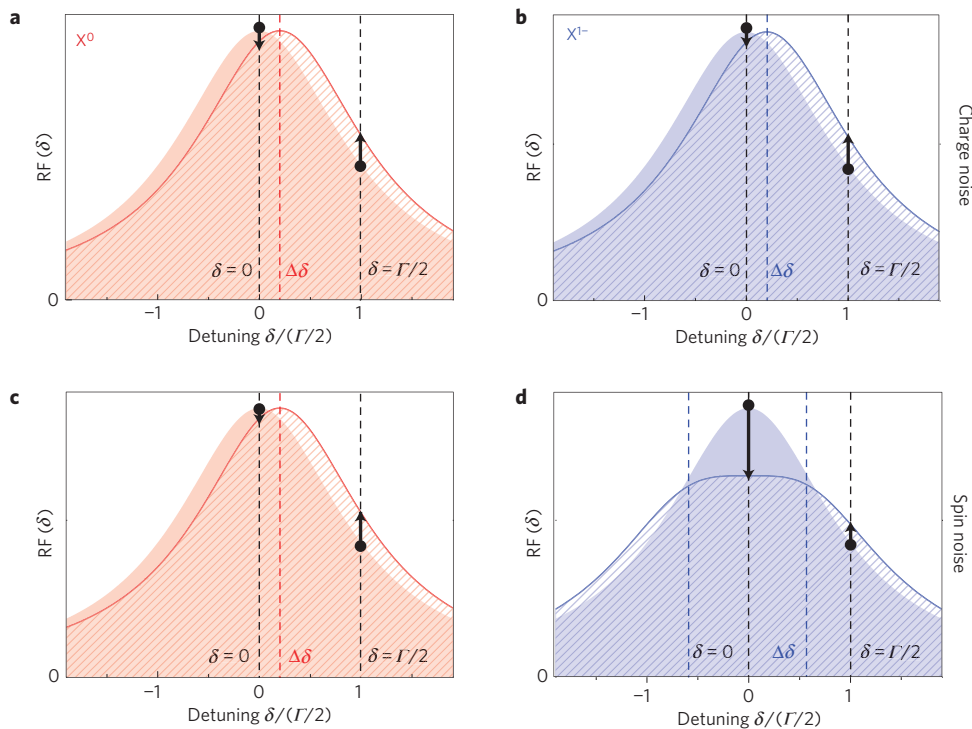
Figure 3 | Distinguishing between charge noise and spin noise. a–c, Schematic showing the effect of charge noise and spin noise on the neutral, X^0, and charged, X^{1-}, excitons (applied magnetic field zero). Charge noise (noise in the local electric field) results in a rigid shift of the optical resonance leading to a small change in RF for zero detuning $\delta = 0$ and a large change in RF at $\delta = \Gamma/2$. This applies for both X^0 and X^{1-} (**a,b**). Without an external magnetic field, spin noise (noise in the local magnetic field experienced by a conduction electron) results in a small shift in the X^0 resonance position, qualitatively as for charge noise (**c**). **d,** For X^{1-} however, spin noise induces a Zeeman splitting in the resonance, resulting in a large change in RF at $\delta = 0$ and a small change in RF at $\delta = \Gamma/2$ (zero for $\delta = \Gamma/2\sqrt{3}$), opposite to charge noise. This difference (a rigid shift of the X^{1-} resonance from charge noise; a breathing motion in the X^{1-} resonance from spin noise) allows charge noise and spin noise to be identified.

the experiment itself and not just the quantum dot is a source of noise, mostly shot noise. However, this experimental noise is highly reproducible. We record its spectrum carefully and, using a protocol (see Supplementary Information) subtract it from the total noise to determine the noise power of the normalized RF signal, $N_{QD}(f)$.

Charge noise versus spin noise

$N_{QD}(f)$ is shown in Fig. 2a. In this case, the gate voltage V_g is set so that the quantum dot contains a single electron and the laser drives the trion resonance, X^{1-}. Two features can be made out in the noise spectrum, a roll-off-like spectrum with high power and low characteristic frequency, and a roll-off-like spectrum with low power and high characteristic frequency. This points to the presence of two noise sources in the semiconductor.

To identify the two noise sources, we present noise spectra taken with two detunings, one with detuning averaged over the experiment zero $\langle\delta\rangle = 0$, the other with average detuning half a linewidth, $\langle\delta\rangle = \Gamma/2$, Fig. 2a. Switching from $\langle\delta\rangle = 0$ to $\langle\delta\rangle = \Gamma/2$ causes the noise power of the low-frequency component to increase by about one order of magnitude and the power of the high-frequency component to decrease (by about a factor of three at a few kilohertz; Fig. 2a). This crucial information allows the nature of the noise, charge or spin, to be identified.

As the local electric field F fluctuates, the detuning δ of the quantum-dot optical resonance with respect to the constant laser frequency fluctuates on account of the d.c. Stark effect. For small electric field fluctuations, the Stark shift is linear: the optical resonance shifts rigidly backwards and forwards on the detuning axis, as shown in Fig. 3a,b. The response in the RF to charge noise has a first-order component in electric field for $\delta = \Gamma/2$ giving rise to large changes in the RF. Conversely, for $\delta = 0$ the first-order

component vanishes. Sensitivity to charge noise in the RF is therefore weak for $\langle\delta\rangle = 0$ yet strong for $\langle\delta\rangle = \Gamma/2$. Spin noise results in a complementary behaviour in the absence of an external magnetic field, $B = 0$. Fluctuations in the local magnetic field B_N arising from spin noise do not shift the X^{1-} resonance backwards and forwards. Instead, a typical B_N fluctuation induces a sub-linewidth Zeeman splitting of the X^{1-} resonance, as shown in Fig. 3d. An oscillatory B_N results in a breathing motion of the RF spectrum. Sensitivity to spin noise in the RF is therefore strong for $\langle\delta\rangle = 0$, and weak for $\langle\delta\rangle = \Gamma/2$. The crucial point is that, for X^{1-} at $B = 0$, the dependence of the RF noise on $\langle\delta\rangle$ is opposite for charge noise and spin noise.

Applying this concept to the quantum-dot response in Fig. 2a leads to the unambiguous conclusion that the noise at low frequencies arises from charge noise and that the noise at high frequencies arises from spin noise. The noise spectrum at $\langle\delta\rangle = 0$ measured on an empty quantum dot, driving the neutral exciton X^0 transition, also shows two noise features, again charge noise and spin noise (Fig. 4a). The X^0 and X^{1-} have similar levels of charge noise. This is expected as the X^0 and X^{1-} d.c. Stark shifts are similar and each exciton probes exactly the same environment. The X^0 spin noise is less however. Part of the explanation is that the X^0 splits into two states even at $B = 0$ (the so-called fine structure, a consequence of an anisotropy in the electron–hole exchange) such that the dispersion for small B_N is quadratic and not linear, reducing massively the sensitivity of X^0 to spin noise (see Supplementary Information).

The noise behaviour X^0 versus X^{1-} supports the charge/spin assignment of the noise processes. Further confirmation is provided in Fig. 2b, which shows $N_{QD}(f)$ curves measured on the same quantum dot over the course of the experiment (several months) under nominally identical conditions. There are changes in the low-frequency noise power (up to a factor of 10) but the high-frequency
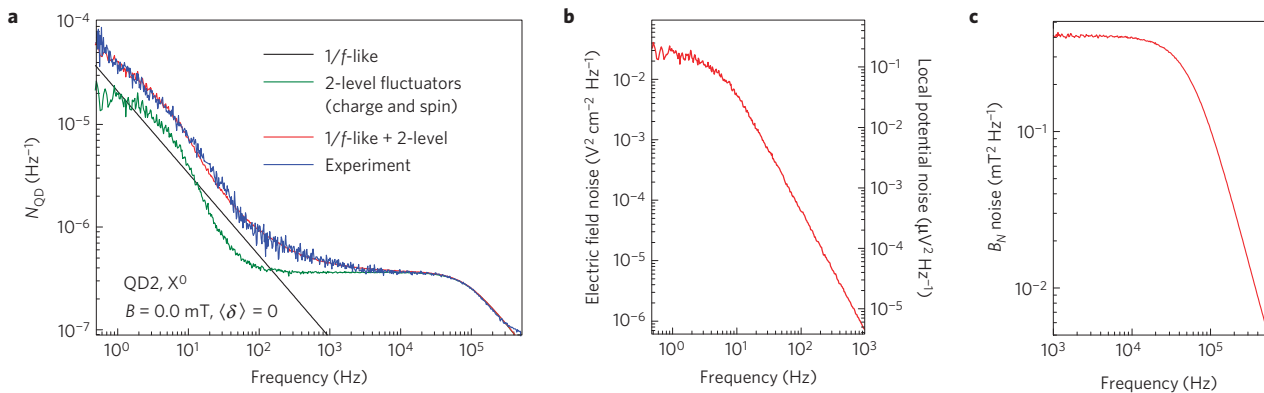
Figure 4 | Noise spectra of local electric and magnetic fields. a, Experimental RF noise spectrum (blue) recorded on the neutral exciton X^0 (same quantum dot as in Figs 1 and 2) with result of simulation (red). The simulation uses parameters $a = 0.032 \, \mu eV \, cm \, V^{-1}$, $N_c = 1.0 \times 10^{10} \, cm^{-2}$, $\tau_0 = 30 \, s$, $\tau_1 = 0.03 \, s$ and $p = 0.1\%$ to model charge noise and $g = -0.5$, $\Delta = 17.3 \, \mu eV$, $N_{eff} = 65$, $A = 90 \, \mu eV$ and $\tau_0 = \tau_1 = 5.5 \, \mu s$ for spin noise (see Supplementary Information). To fully describe charge noise a $1/f^\alpha$ noise component with $\alpha = 0.8$ is added. **b,c**, Local electric field noise (**b**, left y axis), local potential noise (**b**, right y axis) from the two-level fluctuators, and local magnetic field noise (**c**), deduced from the simulations of the RF noise in **a**.

noise remains exactly the same. It is known that the charge state of the sample can change depending on the sample's history: these charge rearrangements result in changes in charge noise at low frequency. The spin noise arises from the host nuclear spins of the quantum dot, which remain the same and retain their properties: this results in the unchanging spin noise at high frequency. Further confirmation in the charge/spin assignment comes from noise spectra in a small B (see Supplementary Information).

Noise levels

Once the noise sources have been identified, the simple rules (see Supplementary Information) connecting RF intensity with the local electric field F (charge noise) and with the local magnetic field B_N (spin noise) allow quantitative statements on the noise to be made. The charge noise has a root-mean-square (r.m.s.) electric field noise $F_{r.m.s.} = 0.46 \, V cm^{-1}$ (bandwidth starting at 0.1 Hz). It is striking that, first, the charge noise is very small: the r.m.s. noise in the local potential is just 1.2 μV. This is a consequence of both the ultrapure material and also the carefully controlled experimental conditions. The sensitivity of the quantum dot to the small levels of charge noise through the Stark effect reflects on the one hand, the potential of quantum dots as ultrasensitive electrometers[7,25,26]; and, on the other hand, the difficulty in generating transform-limited single photons from individual quantum dots. Second, it is striking that the charge noise is concentrated at such low frequencies.

The r.m.s. noise in the Overhauser field measured on X^0 amounts to $B_{N,r.m.s.} = 193 \, mT$ with a characteristic frequency 180 kHz (correlation time 5.5 μs). $B_{N,r.m.s.}$ measured on X^{1-} is smaller, 9 mT, with correlation time 100 μs (see Supplementary Information). The random fluctuations of N nuclear spins lead to a $B_{N,r.m.s.}$ that scales as $1/\sqrt{N}$ (refs 10,11); applied to an InGaAs quantum dot with $N \sim 10^5$, the expectation is $B_{N,r.m.s.} \sim 20 \, mT$ (refs 27,28). On X^0, the large $B_{N,r.m.s.}$ and small correlation time both provide clear evidence that continuous resonant X^0 excitation agitates the nuclear spins. The X^0 and X^{1-} correlation times, a few tens of microseconds, identify the process responsible for the spin noise as the nuclear spin dipole–dipole interaction[10] (see Supplementary Information).

Quantum-dot optical linewidth

A clear result is that both charge and spin noise fall rapidly with increasing frequency such that above 100 kHz, the RF noise power reduces by about 4 orders of magnitude compared with the low frequency limit. The noise curves predict therefore that the exciton dephasing processes are slow relative to radiative decay, which occurs at a gigahertz rate. To explore this, we

measure the X^0 linewidth as the measurement frequency f_{scan} is gradually increased (see Supplementary Information). Figure 2d shows that the RF linewidth Γ decreases from 1.60 μeV to 0.93 μeV as f_{scan} increases from 1 Hz to 50 kHz. At higher f_{scan}, Γ remains constant. Furthermore, within our experimental error (0.1 μeV), this constant value at high f_{scan} corresponds to the transform limit, Γ_0. A transform-limited RF spectrum is shown in Fig. 2c. In other words, the increase in Γ over Γ_0 at low f_{scan} reflects the influence of processes that are slow not just relative to the recombination rate (GHz) but also relative to our maximum experimental speed (100 kHz). These results are confirmed by measuring also X^{1-} with the same procedure. In this case, the linewidth decreases to 0.75 μeV at high scan rates, a lower value than for X^0, reflecting the slightly larger radiative decay time[29] for X^{1-} (see Supplementary Information). We note that the low-frequency X^0 and X^{1-} linewidths are caused by spin noise, not by charge noise: the charge noise implies a line broadening of $<0.05 \, \mu eV$, whereas the $B_{N,r.m.s.}$ values allow us to reproduce both the X^0 and X^{1-} linewidths. Using in this way the low-frequency linewidths as a noise integrator adds weight to our analysis of the noise spectra.

Charge noise and spin noise spectra

The charge noise in $N_{QD}(f)$ is the sum of a Lorentzian spectrum and a $1/f^\alpha$ component with $\alpha \sim 0.8$. The Lorentzian part is characteristic of a two-level fluctuator[30].

A single two-level fluctuator would lead to pronounced telegraph noise in the RF, which we do not observe in this experiment. Instead, we postulate that the Lorentzian noise arises from fluctuations in an ensemble of two-level fluctuators, each with approximately the same transition rates, $0 \rightarrow 1$, $1 \rightarrow 0$. The particular fluctuators are hole localization centres at an interface 150 nm above the quantum dot, identified by the sign and magnitude of very occasional telegraph-like features (see Supplementary Information). This assertion is supported by the fact that the Lorentzian noise disappears when the interface is located much further away from the quantum dots (see Supplementary Information). We note that surplus electrons relax rapidly into the Fermi sea whereas surplus holes, minority carriers, can be trapped in the active part of the device. Electrostatic noise arises on account of fluctuations in the exact configuration of occupied (state 0) and unoccupied (state 1) localization sites in the ensemble. We simulate the noise by taking a fixed array of localization centres, a fixed average hole concentration, a centre-independent capture/escape rate, and a Monte Carlo procedure (see Supplementary Information). The $1/f$-like charge noise is quantum dot dependent with an unknown origin.
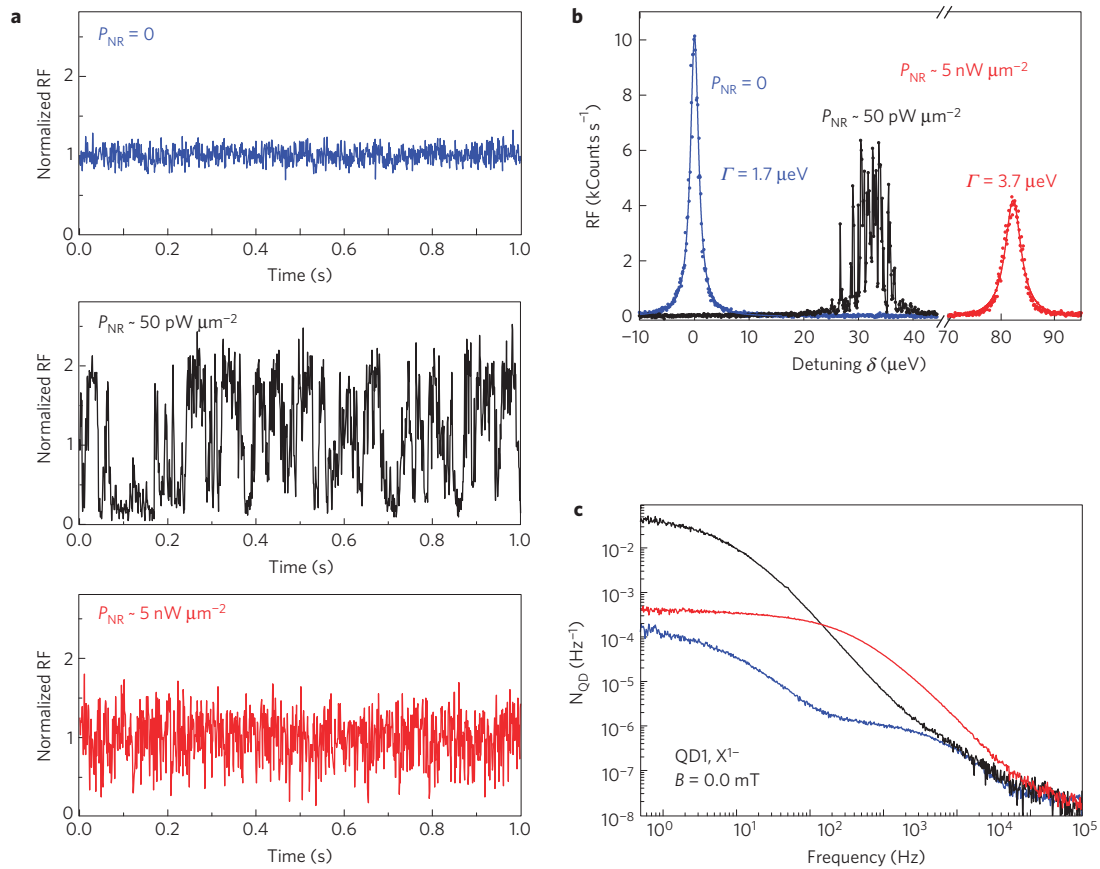
Figure 5 | Noise and above-bandgap excitation. a, Normalized RF time traces from a single quantum dot (same quantum dot as in Fig. 2b). **b,c,** RF spectra (0.1 s integration per point; **b**), and noise spectra plotted for X^{1-} with non-resonant power P_{NR} zero (blue), 1.3 nW (black) and 168 nW (red) focused to a spot area of ~20 μm² (**c**). The non-resonant excitation induces initially considerable noise at low frequencies; larger non-resonant excitation sees the low-frequency noise return close to the value observed without non-resonant excitation but considerable noise now appears above a few tens of hertz.

The spin noise is modelled in a similar way to the Lorentzian charge noise, by treating each nuclear spin as a fictitious two-level system (see Supplementary Information). The simulations yield time traces $F(t)$ and $B_N(t)$. The RF signal $S(t)$ is then calculated according to the known dependence of RF on F and B_N (see Supplementary Information), and then a simulated noise power $N_{QD}(f)$ is calculated using exactly the same routine used to process the experimental data. The complete simulation accounts for simultaneous F and B_N fluctuations; it allows us to draw precise conclusions on the charge and spin noise without assuming for instance an over-simplified dependence of RF on F, B_N; and it enables us to perform a stringent test of the specific charge noise model.

The result of the simulation is shown in Fig. 4a where very close correspondence with the measured noise spectrum has been achieved. The low-frequency noise power, the charge noise, depends sensitively on the number, location and occupation probability of the localization centres; the characteristic roll-off frequency on the capture/escape rates. The high-frequency noise power, the spin noise, depends sensitively on $B_{N,r.m.s.}$; its associated characteristic frequency depends on the nuclear spin flip rate. The success of the simulation allows us to present the noise spectra of F and B_N individually (Fig. 4b,c).

Sample history

It is known that the optical resonance frequency of a particular quantum dot varies slightly from cool down to cool down. Figure 2b shows in addition that the charge noise at low temperature is dependent on the sample's history. The low-frequency noise power varies by up to a factor of ten depending on the particular charge state of the sample. For this particular sample, the low-noise state can be reached by temporary illumination with non-resonant laser light, followed by a wait of a few hours during which the noise at very low frequencies gradually reduces. This information is crucial in optimizing the performance of the device as a spin or optical qubit. The point we stress is that the noise spectrum is much more revealing about the dephasing processes than the optical frequency or optical linewidth alone.

Role of non-resonant excitation

The RF experiment involves driving the optical resonance with coherent laser light at photon energies far below the bandgap of the host semiconductor and the charge noise powers are very small. The situation changes profoundly if RF is detected in the presence of a second laser with photon energy above the bandgap, non-resonant excitation. Even very small non-resonant intensities result in much increased noise. Initially, as the non-resonant power is increased, there is a rapid increase in noise at low frequencies (Fig. 5a) such that the $1/f$-like noise is rapidly swamped. Even measured slowly with 0.1 s integration time per point, there are massive changes in the RF, and, as a consequence, large changes in the exact line shape from scan to scan (Fig. 5b). On increasing the non-resonant power, this low-frequency noise goes away—the noise at the lowest frequencies returns almost to its original level—but noise now appears at higher frequencies (Fig. 5c), in particular between 10 Hz and 10 kHz. Measured slowly, the spectrum acquires a Lorentzian shape without scan-to-scan fluctuations (Fig. 5b), but with an increased linewidth as a consequence of the extra noise at frequencies above 10 Hz. At these non-resonant powers,

the photoluminescence induced by the non-resonant laser is weaker than the RF induced by the resonant laser. At higher non-resonant laser powers, the photoluminescence dominates over the RF and the noise increases further[31]. These results demonstrate that although non-resonant illumination can change and possibly reduce fluctuations at low frequency, it results in a net increase in noise. The standard optical technique, detection of photoluminescence with non-resonant excitation, has this serious flaw, expressed quantitatively in this experiment.

As an outlook, we comment that the high-frequency limit of our experiment is limited only by the photon flux, which can be increased relatively simply using either a micro-cavity or photonic nanowire to enhance the photon extraction efficiency from the device. Our technique is potentially capable of mapping the noise from sub-hertz frequencies up to the gigahertz regime where spin noise corresponding to electron spin precession in B_N may be revealed[10]. The charge noise is measured here in a simple device and represents a baseline for the local charge noise in an ultrapure semiconductor. The noise probe can be applied to micro- or nanostructured devices. The technique opens a new route to probing spin noise. Its dependence on external magnetic field, charge state of the quantum dot, laser excitation and so on can all be probed simply by recording time traces of the RF. The experiment demonstrates that the dephasing processes that limit the T_2^* of the quantum-dot exciton are all slow with respect to radiative recombination; and that charge and spin noise reduce rapidly for increasing frequencies. These results all point to the possibilities of achieving close to dephasing-free qubit operations by working at very high frequencies or at lower frequencies by exploiting echo-like schemes.

Methods

The InGaAs quantum dots are embedded in an ultraclean n-i-Schottky structure with a tunnel barrier of 25 nm and a capping layer thickness of 150 nm. A single-quantum-dot optical resonance is driven in the linear regime with a resonant laser (1 MHz linewidth). Detuning of the quantum dot relative to the constant frequency laser is achieved by tuning the quantum dot through the d.c. Stark effect. RF is detected, rejecting reflected laser light with a dark-field technique[7,18,32]. The arrival time of each photon is recorded over the entire measurement time T.

Post measurement, a binning time t_{bin} is selected, typically 1 μs. The number of counts in each time bin is $S(t)$, the average number of counts per bin $\langle S(t)\rangle$. The fast Fourier transform of the normalized RF signal $S(t)/\langle S(t)\rangle$ is calculated to yield a noise power spectrum, $N_{RF}(f) = |FFT[S(t)/\langle S(t)\rangle]|^2(t_{bin})^2/T$. The quantum-dot noise spectrum $N_{QD}(f)$ is determined from $N_{RF}(f)$ by subtracting the experimental noise (see Supplementary Information). No resonances in $N_{QD}(f)$ have been discovered; thus, we present $N_{QD}(f)$ after averaging at each f over a frequency range yielding equidistant data points on a logarithmic scale.

The quantum-dot optical linewidth Γ is determined by applying a triangle voltage signal to the gate that induces a time-dependent detuning δ. The scan frequency is defined as $f_{scan} = d\delta/dt/\Gamma_0$, where $\Gamma_0 = \hbar/\tau_r$ with τ_r being the radiative lifetime.

The RF depends on the detuning, which in turn depends on the local electric and magnetic fields, $F(t)$ and $B_N(t)$ through a Stark shift and Zeeman effect (see Supplementary Information). Simulations are used to calculate $F(t)$ and $B_N(t)$, adjusting parameters to give the same noise spectrum as in the experiment. The simulations consider an ensemble of independent two-level fluctuators[30], charge localization centres (charge noise) and spins (spin noise).

References

1. Loss, D. & DiVincenzo, D. P. Quantum computation with quantum dots. *Phys. Rev. A* **57**, 120–126 (1998).
2. Petta, J. R. *et al*. Coherent manipulation of coupled electron spins in semiconductor quantum dots. *Science* **309**, 2180–2184 (2005).
3. Shields, A. J. Semiconductor quantum light sources. *Nature Photon.* **1**, 215–223 (2007).
4. Fischer, J. & Loss, D. Dealing with decoherence. *Science* **324**, 1277–1278 (2009).
5. Högele, A. *et al*. Voltage-controlled optics of a quantum dot. *Phys. Rev. Lett.* **93**, 217401 (2004).
6. Atatüre, M. *et al*. Quantum-dot spin-state preparation with near-unity fidelity. *Science* **312**, 551–553 (2006).
7. Houel, J. *et al*. Probing single-charge fluctuations at a GaAs/AlAs interface using laser spectroscopy on a nearby InGaAs quantum dot. *Phys. Rev. Lett.* **108**, 107401 (2012).
8. Klotz, F. *et al*. Observation of an electrically tunable exciton g factor in InGaAs/GaAs quantum dots. *Appl. Phys. Lett.* **96**, 053113 (2010).
9. Pingenot, J., Pryor, C. E. & Flatte, M. E. Electric-field manipulation of the Lande g tensor of a hole in an In(0.5)Ga(0.5)As/GaAs self-assembled quantum dot. *Phys. Rev. B* **84**, 195403 (2011).
10. Merkulov, I. A., Efros, A. L. & Rosen, M. Electron spin relaxation by nuclei in semiconductor quantum dots. *Phys. Rev. B* **65**, 205309 (2002).
11. Khaetskii, A. V., Loss, D. & Glazman, L. Electron spin decoherence in quantum dots due to interaction with nuclei. *Phys. Rev. Lett.* **88**, 186802 (2002).
12. Greilich, A. *et al*. Mode locking of electron spin coherences in singly charged quantum dots. *Science* **313**, 341–345 (2006).
13. Xu, X. *et al*. Coherent population trapping of an electron spin in a single negatively charged quantum dot. *Nature Phys.* **4**, 692–695 (2008).
14. Press, D. *et al*. Ultrafast optical spin echo in a single quantum dot. *Nature Photon.* **4**, 367–370 (2010).
15. Barthel, C., Medford, J., Marcus, C. M., Hanson, M. P. & Gossard, A. C. Interlaced dynamical decoupling and coherent operation of a singlet–triplet qubit. *Phys. Rev. Lett.* **105**, 266808 (2010).
16. De Lange, G., Wang, Z. H., Riste, D., Dobrovitski, V. V. & Hanson, R. Universal dynamical decoupling of a single solid-state spin from a spin bath. *Science* **330**, 60–63 (2010).
17. Bluhm, H. *et al*. Dephasing time of GaAs electron-spin qubits coupled to a nuclear bath exceeding 200 μs. *Nature Phys.* **7**, 109–113 (2011).
18. Matthiesen, C., Vamivakas, A. N. & Atatüre, M. Subnatural linewidth single photons from a quantum dot. *Phys. Rev. Lett.* **108**, 093602 (2012).
19. Nguyen, H. S. *et al*. Ultra-coherent single photon source. *Appl. Phys. Lett.* **99**, 261904 (2011).
20. Urbaszek, B. *et al*. Nuclear spin physics in quantum dots: An optical investigation. *Rev. Mod. Phys.* **85**, 79–133 (2013).
21. Medford, J. *et al*. Scaling of dynamical decoupling for spin qubits. *Phys. Rev. Lett.* **108**, 086802 (2012).
22. Reilly, D. J. *et al*. Measurement of temporal correlations of the overhauser field in a double quantum dot. *Phys. Rev. Lett.* **101**, 236803 (2008).
23. Fink, T. & Bluhm, H. Noise spectroscopy using correlations of single-shot qubit readout. *Phys. Rev. Lett.* **110**, 010403 (2013).
24. Crooker, S. A. & Bluhm, H. Spin noise of electrons and holes in self-assembled quantum dots. *Phys. Rev. Lett.* **104**, 036601 (2010).
25. Alen, B., Bickel, F., Karrai, K., Warburton, R. J. & Petroff, P. M. Stark-shift modulation absorption spectroscopy of single quantum dots. *Appl. Phys. Lett.* **83**, 2235–2237 (2003).
26. Vamivakas, A. N. *et al*. Nanoscale optical electrometer. *Phys. Rev. Lett.* **107**, 166802 (2011).
27. Coish, W. A. & Baugh, J. Nuclear spins in nanostructures. *Phys. Stat. Sol. B* **246**, 2203–2215 (2009).
28. Kloeffel, C. *et al*. Controlling the interaction of electron and nuclear spins in a tunnel-coupled quantum dot. *Phys. Rev. Lett.* **106**, 046802 (2011).
29. Dalgarno, P. A. *et al*. Coulomb interactions in single charged self-assembled quantum dots: Radiative lifetime and recombination energy. *Phys. Rev. B* **77**, 245311 (2008).
30. Machlup, S. Noise in semiconductors—spectrum of a 2-parameter random signal. *J. Appl. Phys.* **25**, 341–343 (1954).
31. Berthelot, A. *et al*. Unconventional motional narrowing in the optical spectrum of a semiconductor quantum dot. *Nature Phys.* **2**, 759–769 (2006).
32. Yilmaz, S. T., Fallahi, P. & Imamoglu, A. Quantum-dot-spin single-photon interface. *Phys. Rev. Lett.* **105**, 033601 (2010).

Author contributions

A.V.K. and J.H. performed the experiments and data analysis with M.P. providing electronics and software expertise. A.L., D.R. and A.D.W. carried out the molecular beam epitaxy; L.G. and A.L. the sample processing. A.V.K. and R.J.W. took the lead in writing the paper. R.J.W. conceived, led and managed the entire project.

Additional information

Supplementary information is available in the online version of the paper. Reprints and permissions information is available online at www.nature.com/reprints. Correspondence and requests for materials should be addressed to A.V.K.

Competing financial interests

The authors declare no competing financial interests.